arXiv:1603.08350v2 [cond-mat.mtrl-sci] 15 Sep 2016

Ab initio Studies on Electronic and Magnetic Properties of X_2PtGa (X = Cr, Mn, Fe, Co) Heusler Alloys

Tufan Roy[1], Aparna Chakrabarti[1,2*]
[1] *Homi Bhaba National Institute, Training School Complex, Anushakti Nagar, Mumbai-400094, India and*
[2] *Indus Synchrotrons Utilization Division,Raja Ramanna Centre for Advanced Technology, Indore-452013, India*

Using first-principles calculations based on density functional theory, we probe the electronic and magnetic properties of X_2PtGa (X being Cr, Mn, Fe, Co) Heusler alloys. Our calculations predict that all these systems possess inverse Heusler alloy structure in their respective ground states. Application of tetragonal distortion leads to lowering of energy with respect to the cubic phase for all the materials. The equilibrium volumes of both the phases are nearly the same. These results of our calculations indicate that all these materials are prone to undergo martensite transition, as has been recently shown theoretically for Mn_2PtGa in the literature. Ground state with a tetragonal symmetry of these materials is supported by the observation of soft tetragonal shear constants in their cubic phase. By comparing the energies of various types of magnetic configurations of these alloys we predict that Cr_2PtGa and Mn_2PtGa possess ferrimagnetic configuration whereas Fe_2PtGa and Co_2PtGa possess ferromagneic configuration in their respective ground states.

PACS numbers: 71.15.Nc, 71.15.Mb, 81.30.Kf, 75.50.Cc

I. INTRODUCTION

Full Heusler alloys (FHA) have drawn considerable attention of the researchers as some of them show shape memory alloy property. In this family, Ni_2MnGa is the most studied prototype ferromagnetic shape memory alloy. It is reported that Ni_2MnGa shows large magnetic field induced strain (MFIS) as well as magnetoresistance effect (MRE), which makes Ni_2MnGa a potential material to be used as sensors, actuators etc.[1–3] However, the basic drawbacks of this material in terms of technological application are its brittleness and the low martensite transition temperature (T_M which is 210 K)[4], because from the application point of view, it is mandatory that T_M should be above room temperature. In the literature, it is reported that, for this type of FHA systems, the T_M, Curie temperature (T_C) as well as the inherent crystalline brittleness (ICB) are highly dependent on the composition. Hence, there is a vast amount of work searching for new Heusler alloys with improved properties, which include low ICB, as well as T_M and T_C above room teperature. This is important from the point of view of technological application, for example, as actuators, sensors etc.[5–14] There are also some shape memory alloys found in the literature which are termed as high temperature shape memory alloys (HTSMA), whose martensite transition temperature is above about 120°C (i.e. 393 K) and they find their application in engines of automobiles, turbines, airplanes etc.[15–18]

There is another class of FHAs which is seen to be half metallic in nature.[19] In this kind of Heusler alloys, density of states of either the majority or the minority spin vanishes at the Fermi level and these materials have potential application as spintronic devices. Generally, many of the Co-based Heusler alloys exhibit this behaviour, like, Co_2CrGa, Co_2MnGa, Co_2MnSn.[20,21] However, some metallic Co-based materials, like, Co_2NbSn, Co_2NiGa are found to exhibit shape memory alloy property.[22–27] Hence, it may be worth probing if there are Co-based Heusler alloys which show both the properties i.e. shape memory property as well as high spin polarization at the Fermi level. One such material, Co_2MoGa, has recently been predicted by us.[23]

Currently, Co_2NiGa and related alloys have gained interest among the researchers. Some of these have been studied in detail theoretically[24,25] as well as have already been prepared experimentally.[26,27] Interestingly, Co_2NiGa shows the shape memory alloy property as well as it possesses different (inverse Heusler alloy) structure compared to many of the Co-based systems, which are known to exhibit half-metallicity and have the conventional Heusler alloy structure in their ground state. It is to be further noted that, the Co-based materials possess reasonably high Curie temperature. All these above-mentioned findings in the literature have motivated us to probe the Co_2NiGa-derived Heusler alloy systems. It is to be further noted that, in a very recent work[13] it has been shown that, substitution of Ni by Pt in case of Ni_2MnGa reduces the inherent crystalline brittleness as well as it makes the tetragonal state more stable compared to its cubic phase. Besides that, Mario et al have observed an enhancement of T_C in case of Co doping in the Pt based systems.[10] So, studying the literature[10,13,28], we can expect that, the effect of replacement of Ni by Pt on various physical properties of Co_2NiGa may turn out to be interesting both from fundamental as well as application

* Electronic mail: aparnachakrabarti@gmail.com

points of view.

Furthermore, number of valence electrons of the system has been shown to play an important role in determining the properties of these alloy systems. In this work, therefore, we have discussed the changes in the magnetic, electronic as well as mechanical properties of X_2PtGa as X is varied and the number of valence electrons of the X element, which is a first row transition metal atom (TM), changes systematically (X being Cr, Mn, Fe, Co). Among these materials Mn_2PtGa is already experimentally prepared and theoretically studied.[29–32] It shows an inverse Heusler alloy structure and possesses a ferrimagnetic configuration as is the case for Mn_2NiGa.[33] We compare our calculated results with the data in the literature, wherever available. In what follows, first, we give a brief account of the method we used and then we present the results and discussion. In the end, the results of this work are summarized and conclusions are drawn.

II. METHOD

The geometry optimization of all the materials have been carried out using Vienna Ab initio Simulation Package (VASP)[34] where the projector augmented wave method (PAW)[35] is implemented. For the exchange-correlation functional, generalized gradient approximation has been used over local density approximation.[36] We have used the energy cut-off for plane wave expansion of 500 eV. The calculations of energies have been performed with a k mesh of 15×15×15 for the cubic case and for the tetragonal phase also we have used similar kind of k mesh. All the calculations have been carried out with the energy and the force tolerance were 10 μeV and 10 meV/Å, respectively. For cubic crystals there are three independent elastic constants namely C_{11}, C_{12} and C_{44}. To find these three independent constants we have applied three different kind of strains on the geometrically optimized cubic structure of the respective systems using VASP code. These strains are (δ, δ, δ, 0, 0, 0)(e_1), (0, 0, δ^2/(1- δ^2), 0, δ)(e_2) and (δ, δ, $(1+\delta)^{-2}$-1, 0, 0, 0)(e_3). The applied strain should be as small as possible; in our case we have applied strain varying from 0.02 to -0.02 in steps of 0.005.

It is well known that, all-electron calculations are more reliable for the prediction of magnetic properties particularly for the systems containing first row transition elements. Hence, we have carried out all electron spin polarized relativistic calculations on the optimized geometry for all the systems using full potential linearised augmented plane wave method (FPLAPW).[37] For exchange-correlation functional, generalized gradient approximation (GGA)[36] over local density approximation is used. An energy cut-off for plane wave expansion was used of about 16 Ry ($R_{MT}K_{max}$ = 9.5). The cut-off for charge density was G_{max}=14. The number of k points in the self-consistent-field calculation is 8000 (256) in the cubic case, whereas for the tetragonal case the number is 8000 (635) in the reducible (irreducible) Brillouin zone (BZ). To get detailed insight about the magnetic interaction between the constituent atoms, we have used spin-polarized-relativistic Korringa-Kohn-Rostoker method (SPRKKR) as implemented in SPRKKR package[38], which provides the Heisenberg exchange coupling constants (J_{ij}). From J_{ij} we have calculated T_C following the approach of Liechtenstein et al.[39] The SCF calculations have been carried out with the local density approximation as the exchange-correlation potential and a k mesh of 21×21×21 in the BZ were used and further an angular expansion upto $lmax = 3$ was considered for each atom.

III. RESULTS AND DISCUSSION

A. Geometry Optimization, Electronic Stability and Possibility of Martensite Transition

Geometry Optimization - FHAs in the cubic phases crystallize in two types of crystal structures, namely, conventional Heusler alloy structure and inverse Heusler alloy structure. In case of FHA there are four fcc sublattices centered at (0.25, 0.25, 0.25), (0.75, 0.75, 0.75), (0.50, 0.50, 0.50), (0.00, 0.00, 0.00), which we label as A, B, C and D sublattices, respectively. In case of a conventional Heusler alloy structure (with a formula X_2YZ), the X atom occupies the A and B sublattices, the Y atom occupies the C sublattice and D sublattice is occupied by the Z atom. This X_2YZ structure shows a $Fm\bar{3}m$ (number 225) space group. On the other hand, in case of inverse Heusler alloy structure (with a formula XYXZ), X atom occupies the A and C sublattices and they are termed as X2 and X1, respectively, Y atom occupies the B sublattice whereas the Z atom occupies the D sublattice. This XYXZ structure assumes a $F\bar{4}3m$ (number 216) space group. Full geometry optimization has been carried out for both the possibilities for all the materials.

Electronic Stability and Ground State Magnetic Configuration - For all the systems studied here (X_2PtGa, X being Cr, Mn, Fe, Co), the formation energies in the cubic structure have been calculated and compared (Table 1) for both inverse and conventional Heusler alloy structure with different magnetic configurations to probe the ground state of these systems both in terms of crystal structure and the magnetic configuration. We have considered three

Table 1. Comparison of formation energies between inverse and conventional Heusler alloy structure with different magnetic configurations. Lattice parameters after geometry optimization are also reported.[a]

Material	Crystal structure	Magnetic Configuration	Formation Energy (kJ/mol)	a_{init}(Å)	a_{opt} (Å)
	Inverse	FM	-62.63(converged to FIM)	6.10	6.10
	Inverse	FIM	**-62.63**	6.10	6.10
Cr_2PtGa	Inverse	NM	+2.88	6.10	5.99
	Conventional	FM	+6.36	6.10	6.22
	Conventional	NM	+68.92	6.10	6.03
	Inverse	FM	-72.75	6.13	6.15
	Inverse	FIM	**-117.67**	6.13	6.13
					6.13[b]
Mn_2PtGa	Inverse	NM	+25.45	6.13	5.93
	Conventional	FM	-71.29	6.10	6.21
	Conventional	NM	+45.98	6.10	5.94
	Inverse	FM	**-99.58**	6.00	6.00
	Inverse	FIM	-36.98	6.00	6.02
Fe_2PtGa	Inverse	NM	+47.89	6.00	5.91
	Conventional	FM	-29.46	6.00	6.02
	Conventional	NM	+37.67	6.00	5.91
	Inverse	FM	**-58.83**	5.95	5.95
	Inverse	FIM	-23.22	5.95	5.89
Co_2PtGa	Inverse	NM	-12.72	5.95	5.90
	Conventional	FM	-46.57	5.95	5.93
	Conventional	NM	-14.35	5.95	5.90

[a]Comparison with experiments or previous calculations, wherever data are available
[b]Ref.32

different kinds of magnetic configurations. These are with long-range ferromagnetic (FM), ferrimagnetic (FIM) and nonmagnetic (NM) ordering. For FM configuration, all the moments of the X and Pt atoms are parallel to each other. Under FIM configuration, there is one type of magnetic configuration possible, in case of conventional Heusler alloy structure, where X and Pt atoms are anti-parallel to each other. In this case, FIM type of magnetic configuration is found to converge to the FM configuration of the respective structure. So, consequently, we have not included any results corresponding to this magnetic structure (FIM) in Table 1. In case of inverse Heusler structure, under FIM configuration, there are actually three types of magnetic configurations possible. This is because the X1 and X2 atoms are occupying crystallographically inequivalent sites. In the first case (FIM-1), the moment of Pt atom is taken to be anti-parallel to the X atoms (both X1 and X2 atoms are parallel to each other). Another ferrimagnetic configuration (FIM-2) is that where moments of X1 and X2 are anti-parallel to each other and the moment of Pt is parallel to X2. The third ferrimagnetic configuration (FIM-3) is that where moments of X1 and X2 are anti-parallel to each other again and the moment of Pt is parallel to X1. However, the FIM-1 configuration converges to the corresponding FM structure. FIM-2 and FIM-3 turned out to be energetically same for all the systems. As a consequence, for the inverse structure, we are only reporting the results of FIM-3 configuration in the table and for the latter part of the discussion (expressed as FIM hereafter). In Table 1, we also report the initial guess value of lattice parameter (a_{init}) which has been chosen from the literature in case of Mn_2PtGa. For the rest of the materials probed (i.e. Cr_2PtGa, Fe_2PtGa and Co_2PtGa), a_{init} has been chosen intuitively. In the same table, the optimized lattice parameter (a_{opt}) for each material after full geometry optimization (i.e. relaxing atom positions, unit cell volume and shape) has also been reported. More negative value of formation energy in case of inverse Heusler alloy structure, compared to their respective conventional Heusler alloy structure, suggest that all the systems possess inverse Heusler alloy structure, which is consistent with the valence electron rule.[40] For Cr_2PtGa and Mn_2PtGa, inverse Heusler alloy structure with FIM configuration and for Fe_2PtGa and Co_2PtGa the inverse structure with FM configuration possess the lowest formation energy, hence these configurations are electronically more stable compared to the other combinations. Further calculations are carried out on these structures only.

Possibility of Martensite Transition - Heusler alloys may have the potential to be used as shape memory alloy device if they undergo a structural phase transition, namely martensite transition, from the (low temperature) non-cubic phase to a (high temperature) cubic phase above a certain temperature. This transition requires that the non-cubic phase must have lower energy compared to the cubic phase. We have applied tetragonal distortion on the cubic

system to probe whether there is a lowering of energy with respect to the cubic phase in their respective ground state magnetic configuration. A global minimum has been observed for all the materials at $c/a > 1$ (c is the lattice parameter along z axis and a is the same along x or y direction) as shown in Figure 1. It is also seen that the relative volume change between the cubic phase and tetragonal phase is nominal (Table 2). It is to be noted here that the magnetic configuration for both the cubic and tetragonal phase has been found and taken to be the same in our calculations. Now we discuss in detail about how we arrive at the volume change between the cubic (austenite) phase and the tetragonal (martensite) phase as reported in Table 2. We first consider the fully optimized lattice parameter (Table 1) and assume both the cubic and tetragonal phase have the same volume. Then we vary the ratio of c and a keeping the volume same as that of the optimized cubic phase (Table 1). If a system shows lowering of energy for $c/a > 1$, then we obtain the value of that particular c/a for which energy of the system is lowest. Next, we vary the volume of the tetragonal phase keeping that same c/a. From there we get a variation of energy as a function of total volume of the tetragonal phase. The volume for which the energy of the tetragonal phase is minimum we consider this as the equilibrium volume of the tetragonal phase. Then we calculate the relative change in volume between the optimized cubic and tetragonal phase, which only we report in Table 2. All the materials in both cubic and tetragonal phases possess almost same volume. The maximum variation is about 2.6% which is for Mn_2PtGa. This conservation of the volume and a lowering of energy as a result of tetragonal distorion indicate that these materials are likely to show martensite transition.[7,41]

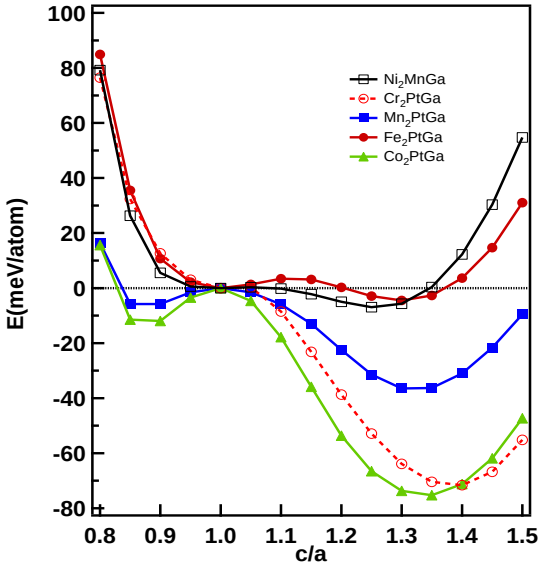

FIG. 1: Variation of the total energy of X_2PtGa (X = Cr, Mn, Fe, Co) systems in their respective ground state magnetic configurations as a function of c/a. Equilibrium c/a values are expected to be around 1.3 to 1.4 for all the systems. The energy of the tetragonal phase has been normalized with respect to the cubic phase of the respective system. Hence, energy E in the Y-axis signifies the energy difference between the cubic and tetragonal phase. Ni_2MnGa is presented as a reference material.

It has been observed in the literature that the martensite transition temperature, T_M, is approximately proportional to ΔE (the energy of the tetragonal phase normalized with respect to the cubic phase) and gives reasonable trend of the T_M across different materials.[7,42] Hence we have used the following equation to calculate the T_M for all these materials.

$$k_B T_M = \Delta E \tag{1}$$

where k_B is the Boltzman constant and we have used the following conversion factor 1 meV = 11.6 K. The calculated T_M values are listed in Table 2. It is found that except Fe_2PtGa, all the alloys are expected to possess a martensite transition temperature which is well above the room temperature and Co_2PtGa yields the maximum value.

B. Magnetic and Electronic Property

Analysis of Magnetic State - In Figure 2 we present the variation of total magnetic moment and partial moments as a function of c/a for all the systems. Table 3 presents the magnetic moments, percentage spin polarizations (P_c and

Table 2. Calculated lattice parameter $(c/a)_{eq}$ and martensite transition temperature[a]

Material	$(c/a)_{eq}$	ΔE(meV/atom)	T_M(K)	$\lvert\Delta V\rvert$/V(%)
Cr_2PtGa	1.41	71.94	834.5	1.00
Mn_2PtGa	1.33	41.06	476.3	2.6
	1.32[b]			3.13[b]
Fe_2PtGa	1.29	4.40	51.0	0.11
Co_2PtGa	1.37	76.43	886.6	1.50

[a]Comparison with experiments or previous calculations, wherever data are available
[b]Ref.32

P_t for cubic and tetragonal phases, respectively) and Curie temperatures (calculated from the Heisenberg exchange coupling parameters as discussed later) of all the magnetic materials in their respective cubic and tetragonal phases. We observe that Cr_2PtGa and Mn_2PtGa are likely to be ferrimagnetic; on the other hand, Co_2PtGa and Fe_2PtGa may possess ferromagnetic ordering, in their respective ground state. The results from the literature, wherever available, have been presented in the same table and it is found that the matching between the data from literature and our calculations is reasonably good. For Cr_2PtGa, the alignment of spin for Cr atom at A sublattice (referred to as Cr2) is opposite to that at C sublattice (referred to as Cr1). Same is observed in case of Mn_2PtGa also, resulting in a ferrimagnetic ground state as in the case of Mn_2NiGa.[33] It is worth mentioning that both Cr and Mn atoms possess anti-ferromagnetic ground state in their bulk forms. So for this type of (inverse Heusler alloy structure) crystal structure, where X atom is the nearest neighbour of itself, the resulting magnetic configuration seems to get influenced by the magnetic configuration of the bulk X atom. This is also the case for the other two materials, namely, Co_2PtGa and Fe_2PtGa. Both these materials have a long-range ferromagnetic ordering and notably both Co and Fe atoms are having ferromagnetic ground state in their respective bulk forms.

Table 3. Calculated magnetic moments and Curie temperatures for both austenite (μ_c, $T_{C,c}$) and martensite phases (μ_t, $T_{C,t}$). In the parentheses of the second and fifth columns, first two values are corresponding to the inequivalent X atoms (X = Cr, Mn, Fe, Co) and the third value corresponds to the Pt atom. P_c and P_t are the percentage of spin polarization at Fermi level for cubic and tetragonal phase, respectively. [a]

Material	$\mu_c(\mu_B)$	P_c(%)	$T_{C,c}$(K)	$\mu_t(\mu_B)$	P_t(%)	$T_{C,t}$(K)
Co_2PtGa	3.25	80.14	584	2.89	71.59	724
	(1.57, 1.60, 0.21)			(1.33, 1.58, 0.14)		
Fe_2PtGa	5.16	1.96	972	5.06	42.34	909
	(2.21, 2.86, 0.23)			(2.32, 2.75, 0.16)		
Mn_2PtGa	0.44, 0.44[b]	24.18, 23[b]	583, 799[b]	0.86, 0.75[b]	20.75, 26[b]	490, 326[b]
	(-3.31,3.60, 0.08)			(-2.76, 3.42, 0.14)		
Cr_2PtGa	1.00	74.39	1500	0.28	5.26	1540
	(-2.21, 2.95, 0.22)			(-2.74, 2.92, 0.04)		

[a]Comparison with experiments or previous calculations, wherever data are available
[b]Ref.32

Electronic Density of States to explain Magnetic States - The origin of the ferrimagnetism in both cubic as well as tetragonal phase for Cr_2PtGa can be understood from the electronic density of states presented in Figure 3. The moments of Cr1 and Cr2 are opposite to each other (Table 3) because of the anti-parallel nature of the spins of Cr1 and Cr2 atoms below Fermi level, which is evident from the partial DOS (Figure 3). The density of states of Cr1 and Cr2 give rise to unequal anti-parallel moments in Cr1 and Cr2 atoms resulting in a ferrimagnetic ground state for Cr_2PtGa. Similar is the case for Mn_2PtGa. Figure 4 gives the total and partial DOS for Co_2PtGa in cubic as well as tetragonal phase. It is clearly seen from the partial DOS of the two Co atoms that the clear exchange splitting observed in case of Cr_2PtGa is not present in case of both the Co atoms of Co_2PtGa. In both materials partial DOS of Pt atoms show: (1) the up and down spin DOS are almost compensated, (2) there is no significant contribution of the DOS near the Fermi level.

Variation of Magnetic Moments as a Function of c/a - To understand the underlying reason behind the variation of magnetic moments as a function of c/a (Figure 2) as well as stability of the tetragonal phase over cubic phases we show the spin polarized total density of states along with DOS of the minority d ($5d$ for Pt and $3d$ for other TM atoms) e_g states near the Fermi level for X1, X2 and Pt atom as a function of c/a. We show these results for two typical materials, namely, Cr_2PtGa and Co_2PtGa in Figure 3 and 4, respectively. The first material is ferrimagnetic and the other one is ferromagnetic in their respective ground state.

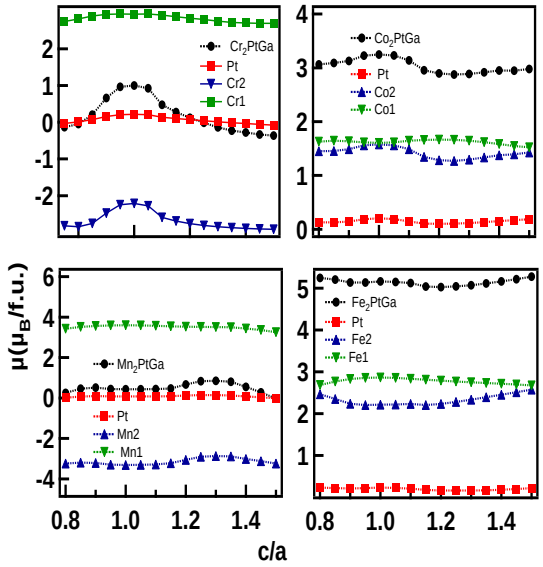

FIG. 2: Variation of the total magnetic moment and partial moments of X_2PtGa (X = Cr, Mn, Fe, Co) systems as a function of c/a.

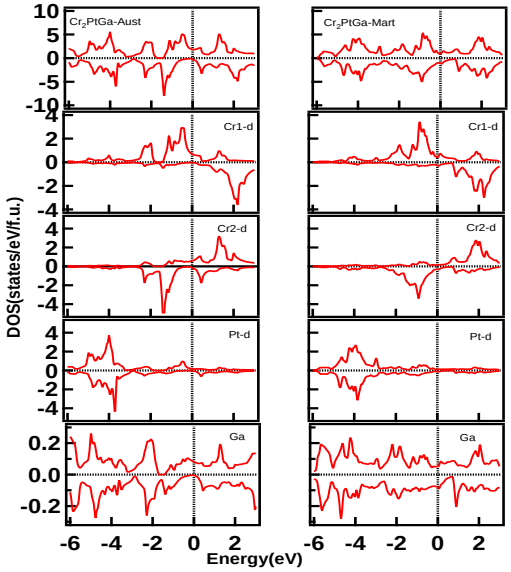

FIG. 3: Spin polarized DOS of Cr_2PtGa (a) Cubic phase (Aust), (b) Tetragonal phase (Mart).

We observe from Figure 2 that there is almost no change in total magnetic moment of Fe_2PtGa as a function of c/a which is also observed for the cubic and tetragonal phases as is evident from the values given in Table 3. For Co_2PtGa we find that, there is a maximum at c/a=1 but in the tetragonal phase the total moment decreases, which can be correlated with the increased distance between Co1 and Co2 atoms resulting in a weaker long-range ferromagnetic interaction between them. On the contrary, for Mn_2PtGa the total moment increases in the tetragonal phase. Being the nearest neighbours to each other, Mn1 and Mn2 atoms are anti-ferromagnetically coupled. Hence, in this case the increased separation between Mn1 and Mn2 makes the anti-ferromagnetic interaction weaker in the tetragonal phase compared to its cubic phase which results in a larger total moment in the tetragonal phase. For Cr_2PtGa the maximum of total magnetic moment at c/a=1 can be correlated with the high spin polarization (75%) at the Fermi level in cubic phase. However, in the tetragonal phase the spin polarization has decreased significantly (5%) as is also

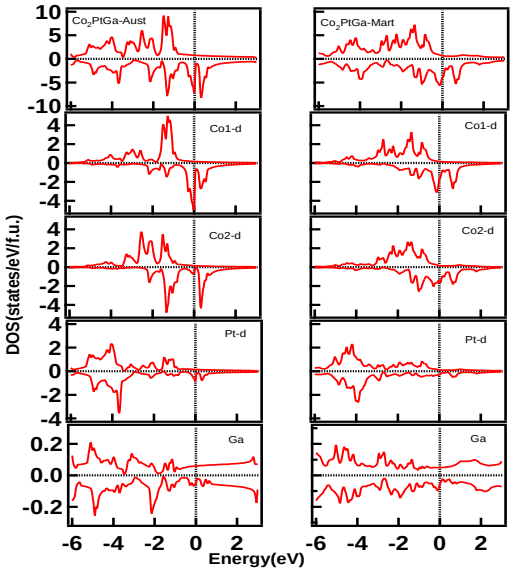

FIG. 4: Spin polarized DOS of Co_2PtGa (a) Cubic phase (Aust), (b) Tetragonal phase (Mart).

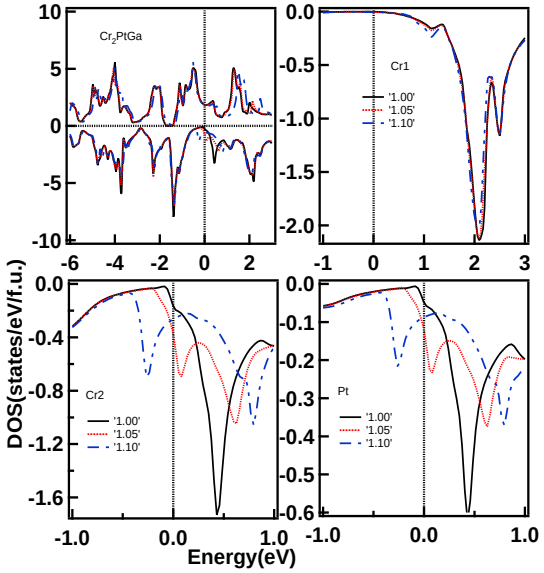

FIG. 5: Spin-polarized DOS of Cr_2PtGa and corresponding minority $3d$ e_g level electrons of Cr1 (top panel), as well as Cr2, and Pt atom (bottom panel) as a function of c/a, maximum value being 1.1.

seen from the corresponding partial moments on Cr1 and Cr2 atoms. This leads to the reduction in the total moment in the tetragonal phase with respect to its cubic phase.

T_C from Heisenberg Exchange Coupling Constants - We observe that in all the cases, the magnetic moment is found to be primarily due to the X atoms as is observed from Table 3. A change in the total magnetic moment between cubic and tetragonal phase is observed. This change is maximum for Cr_2PtGa. Because the total moment is substantially lower in the low temperature phase, both Cr_2PtGa and Co_2PtGa is likely to show an inverse magnetocaloric effect.[43] Next we discuss the Heisenberg exchange coupling paramaters. In Heusler alloys, there is a direct exchange interaction and an indirect RKKY-type of interaction.[44] The prototype shape memory alloy, Ni_2MnGa, which possesses a conventional Heusler alloy structure, a strong ferromagnetic direct interaction exists between Ni and Mn, whereas the interaction between two Mn atoms is of indirect nature.[12,45] In case of Mn_2NiGa, with an inverse Heusler alloy

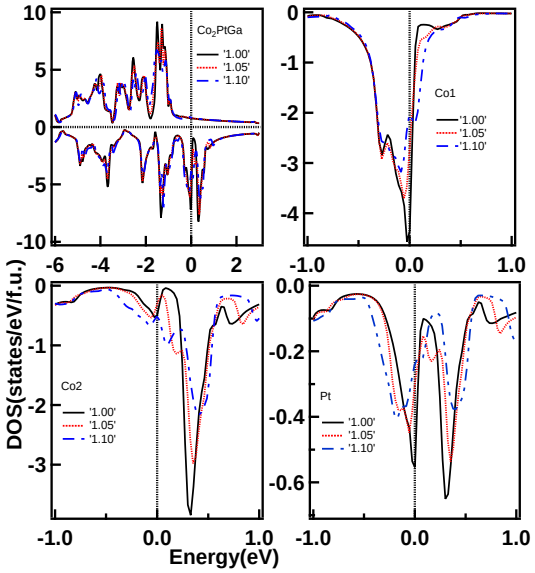

FIG. 6: Spin-polarized DOS of Co_2PtGa and corresponding minority $3d$ e_g level electrons of Co1 (top panel), as well as Co2, and Pt atom (bottom panel) as a function of c/a, maximum value being 1.1.

structure, there is a direct anti-ferromagnetic interaction between the two inequivalent Mn atoms which are nearest neighbours to each other.[33] This interaction is much stronger compared to the direct exchange interaction observed between Ni and Mn in case of Ni_2MnGa. In Figure 7 we present the Heisenberg exchange coupling parameters (J_{ij}) between ith and jth atoms for all the systems X_2PtGa (X = Cr, Mn, Fe, Co) studied here, as a function of inter-atomic spacing between them in their cubic phase. The J_{ij}'s for intra sublattice (X1-X1, X2-X2) and inter sublattice (X1-X2, X1-Pt, X2-Pt) are depicted here. It is quite clear from the plots that in all cases the X1-X2 interaction is the most dominant one and has a crucial role in determining the T_C value of the corresponding material. A weak oscillatory type of indirect exchange interaction is observed for intra sublattice exchange interaction X1-X1 and X2-X2, which is an indication of presence of RKKY type of interaction in the systems.

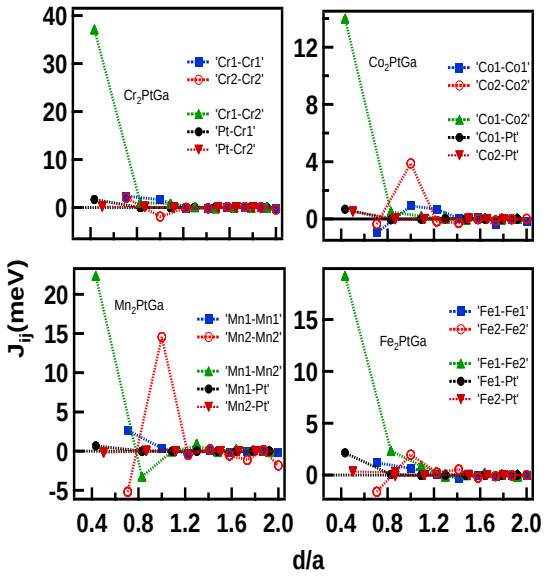

FIG. 7: J_{ij} parameters between different atoms of X_2PtGa as a function of distance between the atoms i and j (normalized with respect to the respective lattice constant).

The Curie temperatures for both the austensite and martensite phases for all the materials have been calculated from the Heisenberg exchange coupling parameters following Ref.39. In literature it has been mentioned that in the mean field approximation, there is an overestimation of Curie temperature.[46–48] It has been argued that in the mean field approximation, spin fluctuations are neglected and the magnetic moments are taken to be more rigid, which causes an overestimation of Curie temperature. It is known that a change in T_C is observed during a structural transition.[32] This has been experimentally observed by Khovailo et al[49] for Ni-Mn-Ga alloy system. This change is because of the differences in the partial moment and interatomic spacing between the two phases. The strength of hybridization between the atoms depends on their separation. This hybridization and the moment of the interacting atoms control the strength of exchange interaction between the atoms[50], and consequently, the T_C of the corresponding system as has been observed from Table 3. The Curie temperatures for all the systems are observed to be much higher compared to the room temperature for the both cubic and tetragonal phases.

Spin Polarization - Table 3 also suggests that the spin polarization (P) at Fermi level for Co_2PtGa is the highest in both the cubic and tetragonal phases compared to all the other materials. This is much higher from the spin polarization of the prototype shape memory Heusler alloy, Ni_2MnGa. This can be understood from Figure 4, which presents the spin projected DOS of cubic as well as tetragonal phase of this material. We can see that in both the cases, the minority spin has a significantly larger contribution to the DOS at the Fermi level compared to the majority spin.

Stabilization of Tetragonal Phase versus the Density of States - The stabilization of the tetragonal phase over the cubic phase of the shape memory Heusler alloys has been argued by the band Jahn-Teller mechanism.[22,51] We have recently shown[23] for a series of Ni and Co-based conventional FHAs, i.e. the X_2YZ type, that the closeness of minority DOS peak of the X atom, with $3d$ e_g symmetry is closely related to the possibility of martensite transition. Here, in this work, all the materials possess inverse heusler alloy structure (XYXZ). A detailed analysis of density of states shows that for these systems the stability of the tetragonal phase over its cubic phase can be correlated with the presence of minority DOS corresponding to the d e_g peak close to the Fermi level for X2 and Pt atom in their respective austenite phase. From Figure 3 we observe that, the Cr2 atom's $3d$ e_g minority DOS peak is located just above the Fermi level (about +0.43 eV). Under tetragonal distortion, this peak is split into two. For c/a=1.10, one part of the peak enters below Fermi level and other part moves above the Fermi level. The same kind of changes is also observed with the Pt $5d$ e_g minority DOS peak which is located at the same energy as Cr2 atom in the cubic phase. This redistribution of density of states for these two atoms leads to the reduction of free energy and to stabilization of the tetragonal phase over the cubic phase. But for Cr1 atom, there is not much change observed in its minority $3d$ e_g density of states under tetragonal distortion.

In case of Co_2PtGa also, we find the same kind of redistribution of minority $3d$ e_g DOS of Co2 and Pt atom under the tetragonal deformation (Figure 4). The single DOS peak of $3d$ e_g minority spin of Co2 atom is observed at +0.33 eV. Under tetragonal deformation this single peak splits into two parts, major part of the peak moves into the higher energy side (+0.35 eV for c/a=1.05) and minor part of the peak moves toward the Fermi level (+0.19 eV for c/a=1.05). Here also we find that there is not much change in the $3d$ e_g DOS of Co1, causing not much of a change in the moment of Co1 atom as a function of c/a. For both the materials Cr_2PtGa and Co_2PtGa, we find that the tetragonal distortion causes the change of peak position of d e_g DOS primarily of the X2 atom and Pt atom. The X2 atom's moment contributes significantly toward the total moment. This is the reason the variation of total moment as a function of c/a follows primarily the variation of mainly X2 atoms moment (Figure 2). For all the materials studied here, we find mimimum change in the moment of X1 as a function of c/a. We note here that Luo et. al.[52] have observed for Mn_2NiGe which is also an inverse Heusler alloy, the variation of magnetic moment of the two in-equivalent Mn atoms follows different trend because of their different chemical surroundings leading to different hybridization effects.

Tetragonal Ground State versus Tetragonal Shear Constant - While we show from the electronic properties, the possibility of the materials to be prone to undergo tetragonal distortion, we now focus on the mechanical properties, specifically the tetragonal shear constant (C'). The elastic constants of all the materials have been calculated in their cubic phase. For the cubic crystal the elastic stability criteria are- $C_{11} > 0$; $C_{44} > 0$; C_{11}-$C_{12} > 0$; $C_{11} + 2C_{12} > 0$.[53] It is observed that all the alloys satisfy these conditions but the 3rd condition is not satisfied by some of the materials. This leads to a negative value of C' for these. Rest of the materials show small positive values of it. This softening of C' indicates the instability of the cubic phase. For the prototype shape memory alloy, Ni_2MnGa, the softening of C' is already observed from experiment.[54] For Cr_2PtGa and Fe_2PtGa, C' is a small positive quantity, with values 7.56 GPa and 11.80 GPa, respectively. On the other hand, Co_2PtGa and Mn_2PtGa exhibit negative values for the same.

Cauchy pressure (C^P) is defined as the difference between C_{12} and C_{44}. The value of C^P indicates the nature of bonding in a system.[55,56] For all the systems studied here C^P is found to be positive. Pugh phenomenologically related the ratio between shear modulus and bulk modulus (G/B) to the inherent crystalline brittleness of a material.[57] In the estimation of shear modulus we have followed the formalism given by Voigt[58](G_V) over given by Reuss[59](G_R). This is because G_R is largely underestimated for the materials which show softening of C'; the reason behind this has been

Table 4. Mechanical properties of the austenite phase of materials

Material	C_{11} (GPa)	C_{12} (GPa)	C_{44} (GPa)	C' (GPa)	B (GPa)	G_V (GPa)	G_R (GPa)	G_V/B	C^P (GPa)	Θ_m(K)± 300
Cr_2PtGa	151.08	135.96	99.86	7.56	141.00	62.94	16.97	0.45	36.90	1445
Mn_2PtGa	120.11	140.67	100.32	-10.28	133.82	56.08	-30.36	0.42	40.35	1262
Fe_2PtGa	190.53	166.93	109.87	11.80	174.80	70.64	25.40	0.40	57.06	1679
Co_2PtGa	140.18	199.71	110.22	-29.77	179.87	54.22	-125.11	0.30	84.49	1381

discussed in detail in our previous work.[13] If the ratio (G/B) is greater than ∼0.57, the corresponding crystalline material is supposed to be inherently brittle. According to our calculations, Co_2PtGa is predicted to possess the lowest inherent crystalline brittleness. The upper panel of Figure 8 shows an inverse linear relationship between C^P and G/B ($= G_V/B$). This inverse linear relationship between these two parameters is already reported in literature for a large number of systems.[13,60] Figure 8 (a) suggests that the ICB of Co_2PtGa is quite low with respect to that of Ni_2MnGa. The bottom panel of Figure 8 shows the variation of G/B as a function of atomic number (Z) of the X atom of X_2PtGa (X = Cr, Mn, Fe, Co). It is to be noted that the value of G/B is lowest for Z = 27, i.e. for Co_2PtGa. In literature[61] it has been mentioned that the materials with lower value of G are likely to undergo shear deformation and become more prone to ductility instead of brittle fracture when strain is applied which leads to a higher inherent crystalline brittleness.

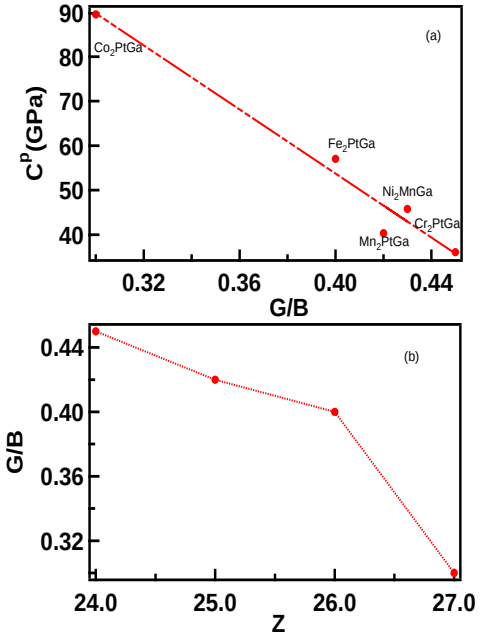

FIG. 8: (a) C^P versus G_V/B plot: A linear fitting has been done, which shows an inverse linear relationship between them. Ni_2MnGa is used as a reference material. (b) G/B versus Z plot. Z is the atomic number of the X atom.

High Melting Temperature of the Studied Systems - For high temperature application of a material, it is mandatory to have very high melting temperatures. Fine et. al.[62] have correlated the elastic constant C_{11} of the cubic metallic as well as interametallic systems with the melting temperature by the following empirical relationship:

$$\Theta_m = 553K + 5.91 \times C_{11}(GPa) \pm 300K \quad (2)$$

Calculated Θ_m values for all the systems (Table 4) are predicted to be sufficiently high for a possible application as SMA even at high temperature, specifically for Co_2PtGa, which is predicted to possess T_M (around 886 K) well above the room temperature.

IV. CONCLUSION

From first-principles calculations, we study the electronic and magnetic properties of X_2PtGa (X being Cr, Mn, Fe, Co) Heusler alloys. We predict a few new materials with Pt being an essential ingredient. By comparing the energies of various types of magnetic configurations, we predict that Cr_2PtGa and Mn_2PtGa possess a ferrimagnetic configuration, whereas, Fe_2PtGa and Co_2PtGa possess a long-range ferromagneic ordering in their respective ground states. Analysing the electronic, magnetic and mechanical properties of all these materials, we predict that, Co_2PtGa, Cr_2PtGa and Fe_2PtGa are found to be three new full Heusler alloy systems, which are likely to show the martensite transition. Among these Co_2PtGa is likely to possess the highest spin polarization at the Fermi level for both the cubic and tetragonal phases. It also exhibits the lowest inherent crystalline brittleness as well as the highest martensite transition (T_M), melting temperature (Θ_m) and Curie temperature (T_C); all of these well above the room temperature.

V. ACKNOWLEDGEMENT

Authors thank P. D. Gupta and P. A. Naik for encouragement throughout the work. Authors thank S. R. Barman and C. Kamal for useful discussion and Computer Centre, RRCAT for technical support. TR thanks HBNI, RRCAT for financial support.

[1] P. J. Webster, K. R. A. Ziebeck, S. L. Town, M. S. Peak, Phil. Mag. B, **49**, 295 (1984).
[2] A. Sozinov, A. A. Likhachev, N. Lanska, K. Ullakko, Appl Phys. Lett. **80**, 1746 (2002).
[3] C. Biswas, R. Rawat, S. R. Barman, Appl. Phys. Lett. **86**, 202508 (2005).
[4] P. J. Brown, A. Y. Bargawi, J. Crangle, K.-U. Neumann, and K. Ziebeck, J. Phys.: Condens. Matter **11**, 4715 (1999)
[5] S. Roy, E. Blackburn, S. M. Valvidares, M. R. Fitzsimmons, S. C. Vogel, M. Khan, I. Dubenko, S. Stadler, N. Ali, S. K. Sinha, J. B. Kortright, Phys.Rev.B **79**, 235127 (2009).
[6] A. Chakrabarti, C. Biswas, S. Banik, R. S. Dhaka, A. K. Shukla, S. R. Barman,Phys. Rev. B **72**, 073103 (2005).
[7] S. R. Barman, A. Chakrabarti, S. Singh, S. Banik, S. Bhardwaj, P. L. Paulose, B. A. Chalke, A. K. Panda, A. Mitra, A. M. Awasthi, Phys.Rev.B **78**, 134406 (2008).
[8] A. Chakrabarti, S. R. Barman, Appl. Phys. Lett. **94**, 161908 (2009)
[9] M. Khan, I. Dubenko, S. Stadler, and N. Ali,J. Phys.: Condens. Matter **16**, 5259 (2004).
[10] M. Siewert, M. E. Gruner, A. Dannenberg, A. Chakrabarti, H. C. Herper, M. Wuttig, S. R. Barman, S. Singh, A. Al-Zubi, T. Hickel, J. Neugebauer, M. Gillessen, R. Dronskowski, P. Entel, Appl. Phys. Lett. **99**, 191904 (2011).
[11] S. Stadler, M. Khan, J. Mitchell, N. Ali, A. M. Gomes, I. Dubenko, A. Y. Takeuchi, A. P. Guimaraes, Appl. Phys. Lett. **88**, 192511 (2006).
[12] A. Chakrabarti, M. Siewert, T. Roy, K. Mondal, A. Banerjee, M. E. Gruner, P. Entel, Phys. Rev. B **88**, 174116 (2013) and references therein.
[13] T. Roy, M. E. Gruner, P. Entel, A. Chakrabarti, J. Alloys Compd. **632**, 822 (2015).
[14] T. Roy, A. Chakrabarti, J. Magn. Magn. Mater. **401**, 929 (2016).
[15] K. Otsuka, X. Ren, Intermetallics **7**, 511 (1999).
[16] J. H. Yang, C. M. Wayman Intermetallics **2**, 111 (1994).
[17] J. V. Humbeek J. Eng. Mater. Technol. **121**, 98 (1999).
[18] J. L. Smailek, R. F. Hehemann, Met. Trans. **4**, 1571 (1973).
[19] R. A. de Groot, F. M. Mueller, P. G. van Engen, K. H. J. Buschow, Phys. Rev. Lett., **50**, 2024 (1983).
[20] H. C. Kandpal, G. H. Fecher, C. Felser, J. Phys. D: Appl. Phys., **40**, 1507 (2007).
[21] J. Kübler, G. H. Fecher, C. Felser, Phys. Rev. B **76**, 024414 (2007).
[22] S. Fujii, S. Ishida, J. Phys. Soc. Jpn., **58**, 3657 (1989).
[23] T. Roy, D. Pandey, A. Chakrabarti Phys. Rev. B. **93**, 184102 (2016).
[24] M. Siewert, M. E. Gruner, A. Dannenbarg, A. Hucht, S. M. Shaprio, G. Xu, D. L. Schlagel, T. A. Lograsso, P. Entel Phys. Rev. B **82**, 064420 (2010).
[25] R. Arroyave, A. Junkaew, A. Chivukula, S. Bajaj, C.-Y. Yao, A. Garay, Acta Mater., **58**, 5220 (2010).
[26] X. F. Dai, G. D. Liu, Z. H. Liu, G. H. Wu, J. L. Chen, F. B. Meng, H. Y. Liu, L. Q. Yan, J. P. Qu, Y. X. Li, W. G. Wang, John Q. Xiao, Appl. Phys. Lett. **87**, 112504 (2005).
[27] J. Dadda, H. Maier, I. Karaman, H. Karaca, Y. Chumlyakov, Scr. Mater. **55**, 663 (2006).
[28] B. Dutta, T. Hickel, P. Entel, and J. Neugebauer, J. Phase Equilib. Diffus.**35**, 695 (2014).
[29] A. K. Nayak, M. Nicklas, S. Chadov, P. Khuntia, C. Shekhar, A. Kalache, M. Baenitz, Y. Skourski, V. K. Guduru, A. Puri, U. Zeitler, J. M. D. Coey, C. Felser, Nature Mater. **14**, 679 (2015)
[30] A. K. Nayak, M. Nicklas, S. Chadov, C. Shekhar, Y. Skourski, J. Winterlik, C. Felser, Phys. Rev. Lett. **110**, 127204 (2013).
[31] A. K.Nayak, R.Sahoo, C. S. Mejia, M.Nicklas, C.Felser, J. Appl. Phys. **117**, 17D715 (2015).

[32] L. Wollmann, S. Chadov, J. Kübler, C. Felser, Phys. Rev. B **92**, 064417 (2015).
[33] S. R. Barman, S. Banik, A. K. Shukla, C. Kamal, Aparna Chakrabarti, Europhys. Lett. **80**, 57002 (2007); S. R. Barman, Aparna Chakrabarti, Phys. Rev. B, **77**, 176401 (2008); G. D. Liu, J. L. Chen,Z. H. Liu, X. F. Dai, G. H.Wu, B. Zhang, and X. X. Zhang, App. Phys. Lett. **87**, 262504 (2005); S. W. D'Souza, T. Roy, S. R. Barman, A. Chakrabarti, J. Phys. : Cond. Matt., **26**, 506001 (2014).
[34] G. Kresse, J. Furthmüller, Phys. Rev. B, **54**, 11169 (1996); G. Kresse, D. Joubert, Phys. Rev. B, **59**, 1758 (1999); VASP 5.2 programme package is fully integrated in the MedeA platform (Materials Design, Inc.) with a graphical user interface enabling the computation of the properties.
[35] P. E. Blochl, Phys. Rev. B **50**, 17953 (1994).
[36] J. P. Perdew, K. Burke, M. Ernzerhof, Phys Rev. Lett. **77**, 3865 (1996).
[37] P. Blaha, K. Schwartz, G. K. H. Madsen, D. Kvasnicka, J. Luitz, WIEN2K, An Augmented Plane Wave plus Local Orbitals Program for Calculating Crystal Properties(Karlheinz Schwarz, Tech. Universitaet, Wien, Austria, 2002, ISBN 3-9501031-1-2).
[38] H. Ebert, D. Kodderitzsch, J. Minar, Rep. Prog. Phys. **74**, 096501 (2011).
[39] A. I. Liechtenstein, M. I. Katsnelson, V. P. Antropov, V. A. Gubanov, J. Magn. Magn. Mater. **67**, 65 (1987).
[40] T. J. Burch, T. Litrenta, J. I. Budnick,, Phys. Rev. Lett. **33**, 421 (1974).
[41] V. V. Godlevsky, M. Rabe, Phys. Rev. B, **63**, 134407 (2001).
[42] M. Siewert, M. E. Gruner, A. Hucht, H. C. Herper, A. Dannenberg, A. Chakrabarti, N. Singh, R. Arroyave, P. Entel, Adv. Eng. Mat., **14**, 530 (2012).
[43] P. J. Von Ranke, N. A. de Oliveira, B. P. Alho, E. J. R. Plaza, V. S. R. de Sousa, L. Caron, M. S. Reis, J. Phys. : Cond. Matt., **21**, 056004 (2004).
[44] M. A. Ruderman and C. Kittel, Phys. Rev., **96**, 99 (1954); T. Kasuya, Prog. Theor. Phys., **16**, 45 (1956); K. Yosida, Phys. Rev., **106**, 893 (1957).
[45] J. Kübler, A. R. Williams, C. B. Sommers, Phys. Rev. B, **28**, 1745 (1983).
[46] E. Şaşıoğlu, L. M. Sandratskii, P. Bruno, Phys Rev B **71**, 214412 (2005)
[47] E. Şaşıoğlu, L. M. Sandratskii, P. Bruno, I. Galanakis, Phys. Rev. B, **72**, 184415, (2005).
[48] J. Rusz, L. Bergqvist, J. Kudrnovský, I. Turek, Phys Rev B **73**, 214412 (2006).
[49] V. V. Khovailo, V. Novosad, T. Takagi, D. A. Filippov, R. Z. Levitin, and A. N. Vasil'ev Phys. Rev. B, **70**, 174413 (2004).
[50] S. K. Bose, J. Kudrnovsk'y, V. Drchal, I. Turek Phys. Rev. B, **84**, 174422 (2011).
[51] S. R. Barman, S. Banik, A. Chakrabarti, Phys. Rev. B, **72**, 184410 (2005) and references therein.
[52] H. Luo, F. Meng, G. Liu, H. Liu, P. Jia, E. Liu, W. Wang, G. Wu, Intermetallics **38**, 139 (2013)
[53] Z. Wu, E.J. Zhao, H.P. Xiang, X. Hao, X.J. Liu, J. Meng, Phys. Rev. B **76**, 054115 (2007) and the references therein.
[54] L. Manosa, A. Gonzalez-Comas, E. Obrado, A. Planes, V. A. Chernenko, V. V. Kokorin, E. Cesari Phys. Rev. B **55**, 11068 (1997).
[55] D. G. Pettifor, Mat. Sci. Tech. **8**, 345 (1992).
[56] M. E. Eberhart, T. E. Jones Phys. Rev. B **86**, 134106 (2012).
[57] S.F. Pugh, Phil. Mag. **45**, 823 (1954).
[58] W. Voigt, Ann. Phys. Chem. N. F. **38** 573 (1889).
[59] A. Reuss, Zeit. Angew. Math. Mech. (ZAMM), **9**, 49 (1929).
[60] H. Niu, X.Q. Chen, P. Liu, W. Xing, X. Cheng, D. Li, Y. Li, Scient. Rep. **2**, 718 (2012).
[61] X.J. Gu, S. J. Poon, G. J. Shiflet, M. Widom, Acta Mater. **56**, 88 (2008).
[62] M. E. Fine, L. D. Brown, H. L. Marcus, Scr. Metall. **18**, 951 (1984).